THE GEOLOGICAL SOCIETY OF AMERICA®

A strong contrast in crustal architecture from accreted terranes to craton, constrained by controlled-source seismic data in Idaho and eastern Oregon

K.K. Davenport[1,*,†], J.A. Hole[1,*], B. Tikoff[2,*], R.M. Russo[3,*], and S.H. Harder[4,*]

[1]DEPARTMENT OF GEOSCIENCES, VIRGINIA TECH, 4044 DERRING HALL, 1405 PERRY STREET, BLACKSBURG, VIRGINIA 24061, USA
[2]DEPARTMENT OF GEOSCIENCE, UNIVERSITY OF WISCONSIN–MADISON, 1215 W DAYTON STREET, MADISON, WISCONSIN 53706, USA
[3]DEPARTMENT OF GEOLOGICAL SCIENCES, UNIVERSITY OF FLORIDA, 241 WILLIAMSON HALL, GAINESVILLE, FLORIDA 32611, USA
[4]DEPARTMENT OF GEOLOGICAL SCIENCES, UNIVERSITY OF TEXAS–EL PASO, 500 WEST UNIVERSITY BOULEVARD, EL PASO, TEXAS 79968, USA

ABSTRACT

Crustal structure was derived from EarthScope Idaho-Oregon (IDOR) controlled-source seismic data across the Precambrian continental margin in the Idaho and Oregon region of the U.S. Cordillera. Refraction and wide-angle reflection traveltimes were inverted to derive a seismic velocity model that constrains the contact between oceanic accreted terranes and craton. The seismic data reveal that the boundary is a near-vertical, through-going feature of the crust, represented by the transpressional western Idaho shear zone (WISZ). The WISZ separates crust with different seismic velocities at all depths, implying a contrast in lithology, and extends to an ~7 km offset of the Moho. The thinner, ~32-km-thick accreted terrane crust to the west is characterized by faster seismic velocities that correspond to an intermediate composition. We interpret a high-velocity layer below a high-amplitude seismic reflection as mafic magmatic underplating associated with the feeder system of the Columbia River Basalts. The cratonic crust east of the WISZ is 37–40 km thick, with a felsic composition to ~29 km subsurface depth, underlain by an intermediate-composition layer above the Moho. The strong contrasts in lithology and crustal thickness across the WISZ have influenced subsequent magmatism and extension in the region. The northwestern extent of the Archean Grouse Creek cratonic block beneath the Atlanta lobe of the Idaho batholith is interpreted based on continuity of crustal architecture in the seismic model. The velocity structure and crustal thickness east of the WISZ are consistent with the Atlanta lobe melting within a thickened crust.

LITHOSPHERE GSA Data Repository Item 2017082 doi:10.1130/L553.1

INTRODUCTION

In western Idaho, a steep tectonic boundary marks the remnants of a suture zone that has been fundamentally reshaped since oceanic-island-arc terranes were accreted during the Jurassic–Cretaceous. This part of the North American Cordillera has undergone a complex sequence of tectonic events that have formed, deformed, overprinted, and altered the crustal structure of the former passive margin. Following subduction and terrane accretion, a period of arc magmatism and intense transpressional deformation consumed much of the suture zone and juxtaposed Precambrian North American craton against relatively juvenile accreted oceanic terranes less than 10 km away (e.g., McClelland et al., 2000; Tikoff et al., 2001; Giorgis et al., 2008). The current demarcation of the intervening boundary is the steeply dipping western Idaho shear zone (WISZ; Fig. 1). Subsequent tectonic events in the region, including the emplacement of the adjacent Idaho batholith, the outpouring of voluminous Columbia River flood basalts, and Basin and Range extension, were influenced by the preexisting crustal architecture.

Kathy Davenport http://orcid.org/0000-0002-9877-4025
*E-mails: Davenport—kd42@vt.edu; Hole—hole@vt.edu; Tikoff—basil@geology.wisc.edu; Russo—rrusso@ufl.edu; Harder—harder@geo.utep.edu.
†Present address: College of Earth, Ocean, and Atmospheric Sciences, Oregon State University, 507 Weniger Hall, Corvallis, Oregon 97331, USA; davenpka@oregonstate.edu

The transition from oceanic-affinity strontium isotope signatures ($^{87}Sr/^{86}Sr \leq 0.704$) to continental-affinity signatures ($^{87}Sr/^{86}Sr \geq 0.708$) typically occurs gradually over >100 km elsewhere in the western Laurentia boundary characterized by suturing (e.g., Giorgis et al., 2005). This isotopic transition occurs over only 5–10 km in Late Cretaceous plutons across the WISZ in the study area (Armstrong et al., 1977; Fleck and Criss, 1985; Manduca et al., 1993). The close proximity of these isopleths indicates a near-vertical contact between the accreted terranes and the North American craton at least to the magma-source depth in the midcrust. However, geochemical data record a second sharp $^{87}Sr/^{86}Sr$ transition in mantle-sourced Miocene volcanic rocks that lie ~120–150 km west of the WISZ in southern Oregon (e.g., Hart, 1985; Leeman et al., 1992; Evans et al., 2002). Models that have been proposed to explain the presence of the two subparallel Sr = 0.706 isopleths involve a detachment crosscutting the WISZ and creating a horizontal offset in the lower crust or upper mantle (Fig. 2; Leeman et al., 1992; Tikoff et al., 2008). Understanding the geometry and implications of this boundary at depth was a primary goal of the multidisciplinary EarthScope IDaho-ORegon (IDOR) project (Tikoff et al., 2017).

The IDOR controlled-source seismic project collected a 430-km-long seismic refraction and wide-angle reflection data set across the WISZ and ~200 km on either side of the boundary (Fig. 1) to constrain seismic velocities in the accreted terranes, Idaho batholith, and craton; determine crustal

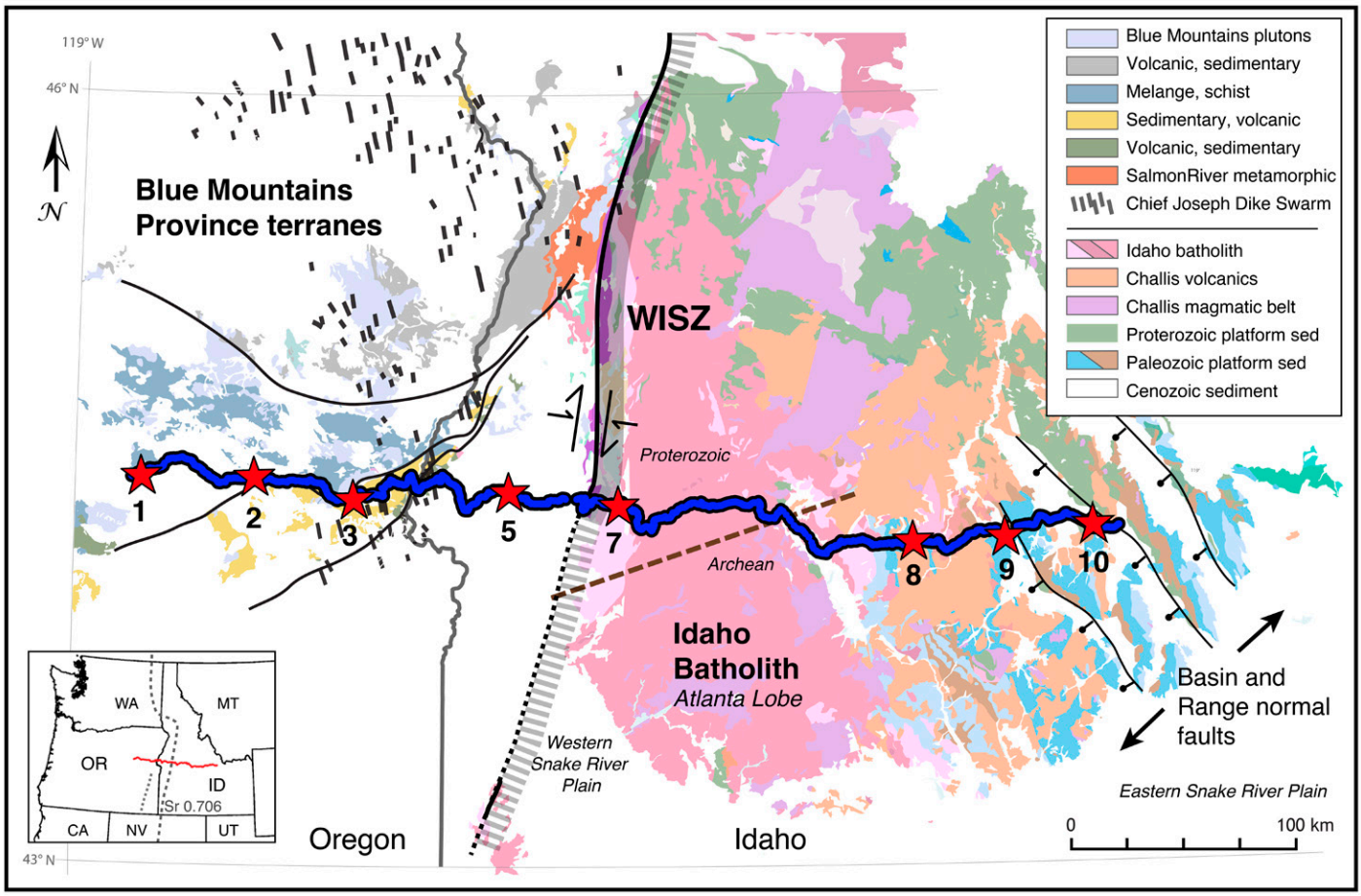

Figure 1. Geologic map of the EarthScope Idaho-Oregon (IDOR) study area in Idaho and eastern Oregon, and the controlled-source seismic profile. Blue dots are seismometer locations; red stars are shot points. WISZ—western Idaho shear zone. The WISZ is not exposed at the surface where line is dashed; gray area indicates approximate surface width of shear zone. The index map shows the $^{87}Sr/^{86}Sr = 0.706$ isopleth. Oregon geology is after LaMaskin et al. (2011, 2015); Idaho geology is after Lewis et al. (2012). Brown dashed line is Archean-Proterozoic boundary based on inherited zircon cores in the Idaho batholith (Gaschnig et al., 2013). State abbreviations: WA—Washington, MT—Montana, ID—Idaho, OR—Oregon, CA—California, NV—Nevada, UT—Utah.

thickness on either side of the boundary; and look for reflections that could be associated with a horizontal detachment structure in the lower crust or uppermost mantle. Results from refraction and reflection traveltime inversion provide new constraints on the deep structure of the boundary between oceanic-arc terranes and the North American craton, and on the structure and seismic velocity (wave speed) of the adjacent crust.

Tectonic and Geologic Background

The modern boundary between the Blue Mountains accreted terranes and Precambrian North American craton in west-central Idaho lies along the steeply dipping, 5–10-km-wide WISZ. Prior to terrane accretion, the western edge of the North American craton had been a dominantly passive margin since the Cambrian (Bond et al., 1984). Since the Jurassic, the margin has undergone multiple phases of tectonic modification associated with the formation of the North American Cordillera and subsequent events, including subduction and terrane accretion, transpressional deformation accommodated by a crustal-scale shear zone, multiple phases of voluminous magmatism, and extension. The complex sequences of events that have modified the Precambrian continental margin in the area of western Idaho and eastern Oregon have culminated in a boundary that is unusually steep and narrow (e.g., Manduca et al., 1993; McClelland et al., 2000; Tikoff et al., 2001; Giorgis et al., 2008).

The sequence of tectonic events that eventually led to the formation of the WISZ began with the amalgamation and accretion of oceanic-arc terranes during the Jurassic and Early Cretaceous (Selverstone et al., 1992; Getty et al., 1993). The accreted Blue Mountains Province terranes (Fig. 1) include oceanic-island arcs and arc-related sedimentary basins amalgamated outboard of North America during the Late Triassic (Vallier, 1977; Brooks, 1979; Dickinson, 1979; Vallier and Brooks, 1995; Dorsey and LaMaskin, 2007), and docked to North America at ca. 160 Ma south of their current location in Oregon and Idaho (e.g., Schwartz et al., 2011; LaMaskin et al., 2015; Gaschnig et al., 2016). The Salmon River suture zone formed by ca. 130 Ma as a result of these accretionary processes along the western edge of the craton (Lund and Snee, 1988; Gray and Oldow, 2005). Estimates for the total northward translation of the Blue Mountains terranes vary from ~100 km to >1000 km (e.g., Wyld and Wright, 2001; Gehrels, 2001; Dickinson, 2004; Housen and Dorsey, 2005; LaMaskin et al., 2011).

After accretion, a subduction-zone continental arc was active in the area of the suture from ca. 120 to 87 Ma (e.g., Manduca et al., 1993; Giorgis et al., 2008; Gaschnig et al., 2010). Strong transpressional deformation

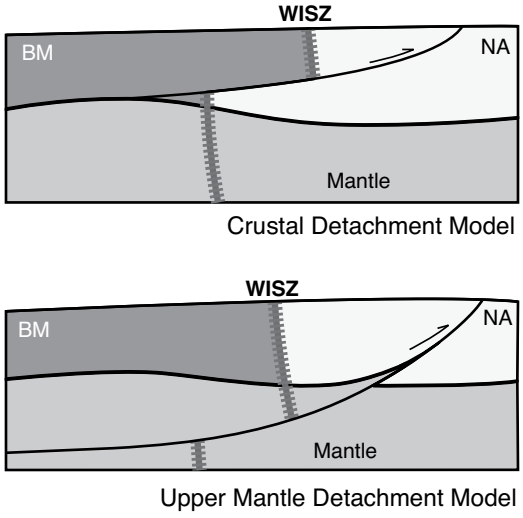

Figure 2. Previous models connecting the surface western Idaho shear zone (WISZ)–Cretaceous $^{87}Sr/^{86}Sr$ = 0.706 isopleth with a lower-crustal source for the Miocene $^{87}Sr/^{86}Sr$ = 0.706 isopleth ~120 km to the west (after Leeman et al., 1992). NA—North American craton; BM—Blue Mountains Province terranes.

produced the Late Cretaceous WISZ within the active continental arc (Fig. 1; e.g., Tikoff et al., 2001; Giorgis et al., 2016). Arc magmatism and the near-vertical shear zone truncated and largely consumed the Salmon River suture zone, producing the sharp Sr isotopic break and resulting in the narrow zone of deformation that represents the modern surface boundary between continental and terrane crust (Lund and Snee, 1988; Manduca et al., 1993; Giorgis et al., 2005). The suture zone and the shear zone are spatially coincident, but they likely represent distinct phases of deformation (McClelland et al., 2000; Tikoff et al., 2001; Giorgis et al., 2008). Remnants of the Salmon River suture zone at the latitude of the IDOR controlled-source seismic line are buried beneath Cenozoic volcanic flows and sediment, but there are exposures of suture-related belt rocks nearby to the north (Fig. 1; e.g., Hamilton, 1963; Gray and Oldow, 2005; Blake et al., 2009). The timing of motion on the WISZ is well constrained by age dates, ductile deformation patterns, and structural relationships in plutons near the shear zone. North of the seismic line, a single pluton exhibits variation from magmatic to solid-state foliations, which constrains initiation of motion on the WISZ to after ca. 104 Ma (Braudy et al., 2016). Cessation of motion is constrained to ca. 90 Ma by U-Pb zircon dating, pluton fabric analysis, and truncation of the WISZ by the Orofino shear zone (e.g., Manduca et al., 1993; McClelland and Oldow, 2007; Giorgis et al., 2008; Benford et al., 2010).

Within and immediately adjacent to the WISZ, the Idaho batholith includes a narrow zone of 110–87 Ma plutons that were coeval with motion on the WISZ (Manduca et al., 1993; Giorgis et al., 2008; Gaschnig et al., 2010). Major- and trace-element geochemistry of this phase revealed components of crust and mantle, indicative of arc magmatism (Gaschnig et al., 2011). A few plutons of similar age also exist further east. The most voluminous parts of the Idaho batholith, however, are the large 83–67 Ma Atlanta lobe, which is crossed by our seismic line, and the smaller 66–53 Ma Bitterroot lobe to the north (Fig. 1; Armstrong et al., 1977; Hyndman, 1983; Vallier and Brooks, 1986; Foster et al., 2001; Gaschnig et al., 2010). The composition of these lobes is more felsic, dominated by peraluminous mica granites, as opposed to the metaluminous amphibole-bearing granodiorite that dominates pre–85 Ma rocks. U-Pb zircon core data indicate that the peraluminous plutons cannibalized earlier plutons and melted the craton (Gaschnig et al., 2010, 2013, 2016). Petrology, metamorphic relationships in the Bitterroot lobe (Foster et al., 2001), and isotope geochemistry (Gaschnig et al., 2011) are all consistent with post–85 Ma melting occurring within thickened continental crust, with little or no contribution from the mantle.

Proterozoic–Paleozoic cratonic platform sediments are exposed to the east of the Idaho batholith near the seismic line (Fig. 1). Cratonic basement rocks are not exposed along the seismic profile, but Gaschnig et al. (2013) observed Archean zircon cores in the southern part of the Atlanta lobe that are consistent with the Grouse Creek unit as defined by Foster et al. (2006) in southern Idaho. U-Pb zircon ages farther north in the Atlanta lobe are consistent with a younger Proterozoic-age cratonic basement similar to that exposed north of the Atlanta lobe. The boundary between these cratonic blocks is poorly defined in the center of the batholith by the geochemical results, but it likely crosses the seismic line obliquely within the Atlanta lobe (Fig. 1).

The tectonic regime in the area became extensional in the Eocene. Eastern phases of the Idaho batholith and cratonic platform sediments are covered by Challis volcanic flows and are intruded by related shallow plutons in central-eastern Idaho (Fig. 1; Hyndman, 1983; Moye et al., 1988; Lewis and Kiilsgaard, 1991; Gaschnig et al., 2010). Challis magmatism spanned 53–43 Ma, with diverse compositions from mixed mantle and crustal sources (Gaschnig et al., 2011). The magmatism has a clear relationship with active extension (e.g., Bennett, 1986; Armstrong and Ward, 1991; Gaschnig et al., 2011).

Large portions of Oregon, Washington, and westernmost Idaho were covered in the Miocene by widespread lava flows of the Columbia River Basalt Group (Fig. 1; Waters, 1961; Reidel and Hooper, 1989; Reidel et al., 2013a, 2013b). Source dikes for the 17–15 Ma Columbia River Basalt flows are restricted to a few areas. The seismic line crosses the major Chief Joseph dike swarm near the Idaho-Oregon border (Fig. 1). The Columbia River Basalts are associated with regional extension and are often attributed to a mantle plume origin (e.g., Camp and Ross, 2004; Hooper et al., 2007; Camp, 2013).

Basin and Range extension, which began ca. 16 Ma (Oldow et al., 1989), dominates the Miocene to ongoing tectonic deformation. The seismic line crosses extensional ranges and valleys in eastern Idaho that strike northwest (Fig. 1), oblique to the northern strike of the Nevada Basin and Range to the south. Extension also occurs in Long Valley immediately east of the WISZ, which has tilted the WISZ to ~70°–80° dip to the east (Tikoff et al., 2001).

IDOR REFRACTION AND WIDE-ANGLE REFLECTION SEISMIC SURVEY

A 430-km-long controlled-source seismic survey was acquired in 2012 across eastern Oregon and Idaho as part of the multidisciplinary EarthScope IDOR project. The east-west refraction and wide-angle reflection profile crosses perpendicular to the boundary separating the Blue Mountains Province accreted terranes and the Precambrian North American craton (Fig. 1). Distance along the profile was sufficient to record seismic waves that sampled the lower crust and uppermost mantle on either side of the boundary. The controlled-source profile was collocated with a broadband teleseismic array deployed as part of the larger IDOR project (Stanciu et al., 2016).

The controlled-source survey included eight explosive shots recorded over two nights. Shot spacing was nominally 40 km, with an ~120 km shot gap across National Forest lands in Idaho due to permitting restrictions.

This gap corresponds to the Idaho batholith, but stations in the batholith and ray paths undershooting the batholith provide reasonable coverage. The shots were each composed of ~900 kg of explosives contained in a 30 cm borehole. The explosive sources were designed to maximize seismic wave generation while minimizing permanent rock deformation, so the explosive medium was buried to an ~21 m center-of-mass depth, and the boreholes were plugged with cuttings and bentonite clay. The wide borehole diameter reduced the vertical length of the medium, increasing the peak pressure of the explosion and thereby increasing seismic energy (Harder et al., 2011).

The shots were recorded at 2555 stations utilizing 4.5 Hz vertical-component geophones and REF TEK 125A "Texan" seismographs recording at a 4 ms sampling rate. The dominant frequency observed from the shots was ~12 Hz. The recording stations were spaced at 100–200 m along roads, 500 m on hiking trails, and ~1 km where access was limited by road closures due to forest fires. There were two gaps of ~5 km each where stations were not deployed due to lack of access by road or hiking trail, and an ~20 km gap on shots 5 and 7 where an encroaching forest fire required stations to be removed prior to the second night of shooting. Instrumentation and field support were supplied by IRIS PASSCAL (Incorporated Research Institutions for Seismology, Portable Array Seismic Studies of the Continental Lithosphere), and deployment was conducted by a field crew of 53, mostly volunteers. An emphasis was placed on education and inclusion during the volunteer selection process, so the field crew included 22 undergraduate students recruited from schools with limited opportunities for research experience, including 4 yr colleges and minority-serving institutions.

SEISMIC DATA

Signal quality varied with the local surface conditions and geology for each source site. The western shots 1, 2, and 3 in Oregon were located in surface outcrops of accreted Blue Mountains Province, overlying Columbia River Basalt volcanics, or overlying Cenozoic sediment (Fig. 1). Source-to-ground coupling for these shots was good due in part to a high water table, and energy from these shots was clearly visible out to the easternmost recording stations, up to 420 km source-receiver offset (Fig. 3). Shot 5 was located in thick basalt flows west of the WISZ in Idaho (Fig. 1). Shot 7 was located on the eastern edge of the WISZ (Figs. 1 and 4). Energy from both of these shots was strongly attenuated in the western ~90 km of the line, likely due to near-surface basins in that region. East of the Idaho National Forest shot gap, shots 8, 9, and 10 provided sources on the cratonic side of the continental margin (Fig. 1). Signal quality for these shots was not as high as the western shots, with usable signal to ~200 km offset (Fig. 5). Shot 8 was located in a water-saturated stream valley near Challis volcanic flows and the eastern extent of the Idaho batholith. Shot 9 was above the water table in unconsolidated alluvial sediments on the western flank of the Lost River Range, which resulted in poor coupling. Shot 10 was located on Proterozoic crystalline rocks at the edge of the Pahsimeroi rift basin. The signal of both shots 9 and 10 was rapidly attenuated by propagation across ridge and valley structures associated with the Basin and Range extension in this area.

Multiple P-wave seismic phases are visible in the shot gathers for each of these shots (Figs. 3–5), as well as S-wave phases that are not considered in this analysis. P-wave phase information is summarized in Table 1. Upper-crust turning waves (Pg) have a high signal-to-noise ratio to 80–100 km offsets on every shot, except shots 9 and 10, which deteriorated beyond 25 and 45 km offset, respectively. The inverse of the time/offset slope of the Pg arrival provides an estimate of the apparent seismic velocity of the layers through which the rays traveled. Very short-offset arrivals for several of the shots show apparent velocities between 3 and 4 km/s, indicating the presence of sedimentary basins. The longer-offset Pg phases on the western side of the line rapidly increase in apparent velocity from ~5.0 km/s for the shallower rays to 6.3–6.4 km/s beyond ~50 km offset (Figs. 3 and 4). On the eastern side of the line, the maximum Pg apparent velocities are 6.0–6.2 km/s to >170 km offset (Figs. 4 and 5). This contrast is most obvious on the shot located at the WISZ, where the slope of the Pg arrivals to the west is visibly different from the slope of the Pg arrivals to the east (Fig. 4). The Pg phase becomes a secondary arrival behind seismic energy refracted from the uppermost mantle (Pn) at offsets greater than 150–160 km for stations west of the shots and ~165–175 km for stations east of the shots. This Pn phase is observable at an apparent velocity of 7.8–8.0 km/s on all shots (Figs. 3–5) except shot 9.

Wide-angle reflections from the midcrust and Moho beneath both the eastern and western portions of the line are observed as secondary arrivals on all of the shots (Figs. 3–5). Reflected phases were identified on shot gathers based on the characteristic quasi-hyperbolic curvature of arrival time as a function of offset ("moveout"), and their largest amplitudes occur near the reflection critical angle. Refractions from below a reflector are tangential to the reflection hyperbola and have an apparent velocity associated with the layer beneath the reflector. Reflections from the Moho (PmP) were identified based on this tangential relationship to the ~8 km/s apparent velocity Pn refracted phase. The Moho reflection observed on shot 7 for stations to the east is unusual in that it is observable at near-vertical angles but has lower amplitude approaching the critical angle. Near-surface features further obscure the association of PmP to Pn on this shot, so the identification of PmP east of the station gap is based on reciprocity with shot 8. PmP traveltimes were only picked in areas where the phase was clearly identifiable.

Reflections from discontinuities within the crust typically have a lower amplitude compared to PmP because the impedance contrast is not as strong as the contrast between crust and mantle. However, on most of the IDOR shots, the PmP arrivals did not have significantly higher amplitude than the intracrustal reflections. This lower amplitude could indicate energy attenuation through the crust, layering at the base of the crust, or a Moho that is gradational at the wavelengths of the data. The largest-amplitude reflection observed in the data is a midcrustal reflection labeled P1P on shot 2 that is much stronger than the Moho reflection (Fig. 3). This reflection is also observed on shots 3, 5, and 7. Midpoints for this arrival are beneath the accreted terranes in Oregon. Modeling indicates that any refracted phase associated with this reflector is not observed because it is not a first arrival and is not detectable in the coda of the Pg and Pn phases. There are two other reflectors observed over a relatively long range of offsets; both are lower amplitude than the P1P reflection. P2P and P3P are both observed before the PmP phase at stations on the eastern side of the line (Figs. 4 and 5). Additional moderate-amplitude reflections are recorded over shorter-offset ranges, including upper-crust reflections observed on shots 2, 7, and 9, midcrust reflections on shots 9 and 10 at the eastern end of the line, and a high-amplitude, short-offset reflection from the lower crust on shot 7 (P4P; Figs. 3 and 4). Arrivals that were reflected from the same intracrustal surface were identified based on reciprocity on reversed shot data.

P-wave traveltimes were picked manually for Pg, Pn, and reflected Moho (PmP) and midcrustal (PxP) phases. Data were filtered using an Ormsby band-pass filter with corner frequencies of 2, 8, 16, and 32 Hz. Crooked road geometry, ~2 km of elevation variation, and narrow near-surface basins produced irregularities in the Pg arrival times of up to 250 ms delay between stations <200 m apart. To correct for these near-station delays, a static time correction based on the first arrival times was temporarily applied to aid picking of secondary arrivals. These time shifts were then removed to obtain absolute traveltimes.

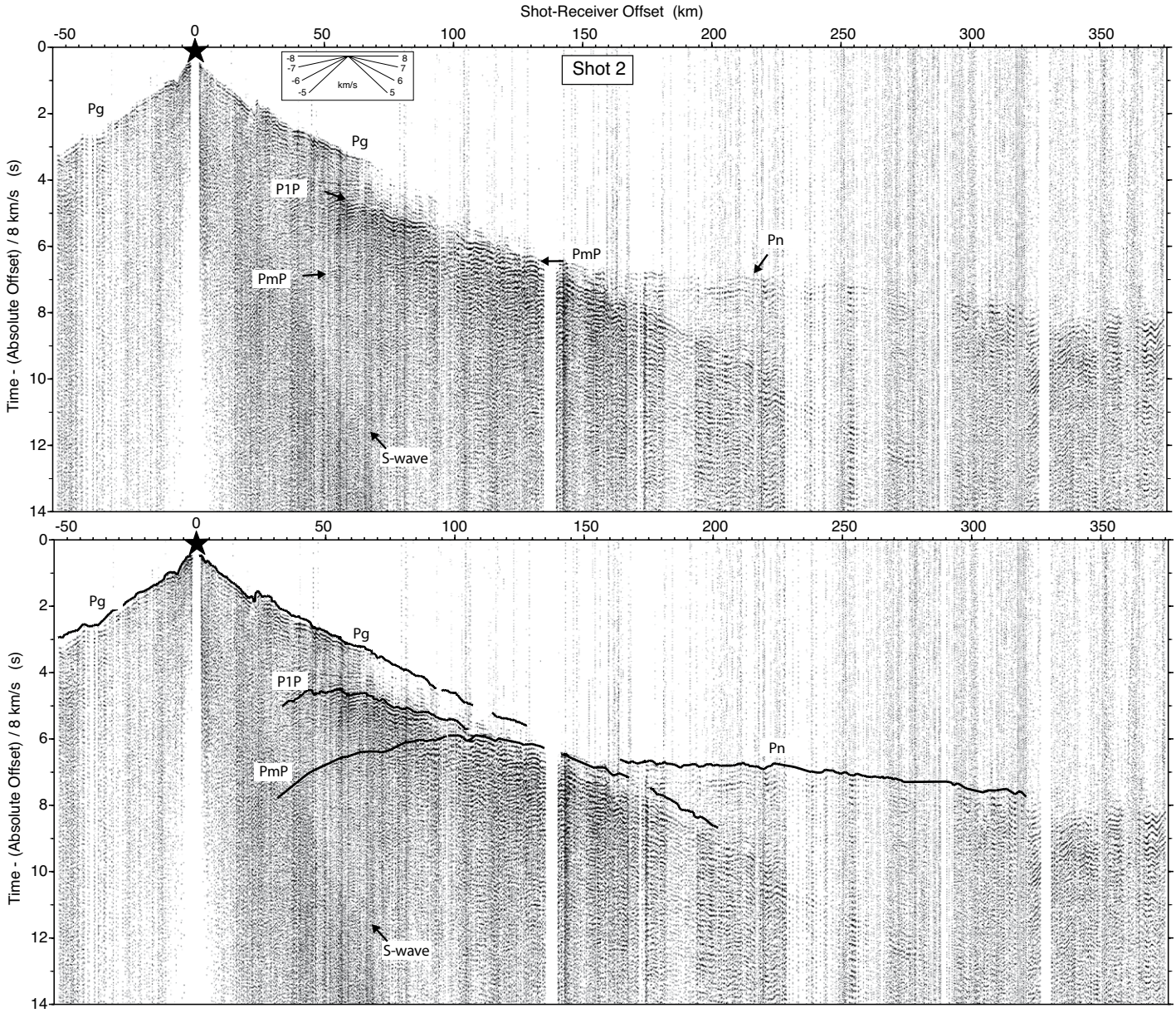

Figure 3. Seismic data shot gather for shot 2 in Oregon with and without phase picks. Time axis is reduced at 8 km/s. Data are band-pass filtered, and trace amplitudes are normalized. See text for description of the labeled seismic arrivals.

The traveltime pick uncertainty on first-arrival Pg picks is estimated to be no more than half of the dominant period (<40 ms) for offsets <50 km on shots 1–8, and <100 ms for shots 9 and 10 due to the near-surface complexities and low-amplitude first arrivals on those shots (Table 1). Longer-offset and secondary arrivals have more variability in the picking uncertainty due to vastly different signal quality, attenuation, and noise on each arrival (Table 1). Secondary arrivals are also subject to a greater chance of cycle skipping (~80 ms/cycle). These picking errors are usually systematic across a range of offsets, and there is a bias toward picking later cycles, and therefore modeling slightly deeper reflector depths, due to the difficulty of identifying emergent energy. Secondary arrivals observed between shots 7 and 8 are most prone to systematic picking errors due to the lack of reciprocity resulting from the lack of shots across this gap. Picks in this region were accepted with higher uncertainty than in other parts of the seismic line to ensure that the large-scale structure modeled beneath the batholith is consistent with the data. Velocities below Pg depths were based primarily on the curvature of midcrustal and Moho reflected arrivals, not their absolute times, so systematic cycle-skipping errors of a few hundred milliseconds on traveltimes of tens of seconds have a minor effect upon velocity.

TRAVELTIME INVERSION

Methodology

Traveltimes of the observed P-wave phases were inverted to produce a seismic velocity model of the crust and uppermost mantle using a three-dimensional (3-D) inversion procedure that incorporates direct, turning,

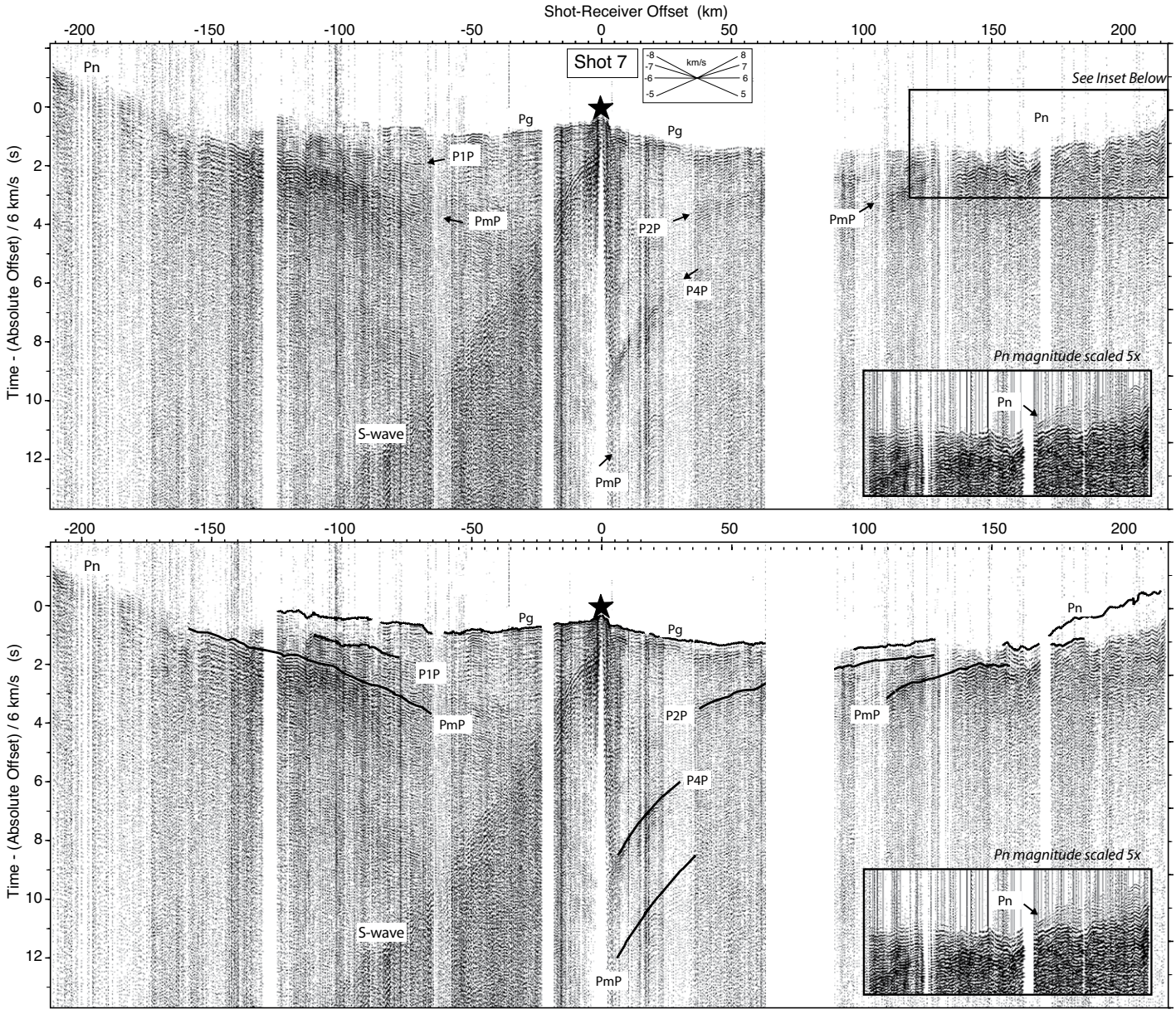

Figure 4. Seismic data shot gather for shot 7, located near the WISZ, with and without phase picks. Time axis is reduced at 6 km/s to emphasize the difference in Pg time and slope across the WISZ. Data are band-pass filtered, and trace amplitudes are normalized. See text for description of the labeled seismic arrivals.

reflected, and refracted arrivals. The method forward models first-arrival traveltimes to every point throughout a gridded 3-D velocity volume using a finite-difference solution to the eikonal equation (Vidale, 1990; Hole and Zelt, 1995). This algorithm is computationally more efficient than ray tracing to a large number of stations. Ray paths through the gridded time volume are found by following the steepest traveltime gradient from the receiver back to the source. Traveltime misfits are inverted by simple back-projection (Hole, 1992), distributing them equally along the ray path. The slowness (inverse of velocity) perturbation of each grid cell is then calculated from the mean misfit of all the rays that intersect that cell. This perturbation volume is smoothed and added to the velocity model. The entire procedure, including ray tracing in the updated model, is repeated until the model reaches an acceptable traveltime misfit.

The algorithm was expanded by Hole and Zelt (1995) and Zelt et al. (1996) to incorporate reflected arrivals by calculating traveltimes through the velocity volume in two steps, where the reflection surface acts as an intermediate "source" for calculating the second part of the ray path. Reflection traveltime misfits are inverted for the depth of the reflector, and then the overlying layer velocity, and iterated until a satisfactory misfit is obtained.

The modeling philosophy emphasizes minimum structure and a layer-stripping approach to building the model. The minimum structure approach (Zelt, 1999) avoids imposed features that are not strictly required by the data, even if a model that includes the imposed structure could be designed to match the data. Long-wavelength velocity structure is determined in the earliest iterations of the modeling process by applying smoothing to the slowness perturbation at a scale that is only slightly

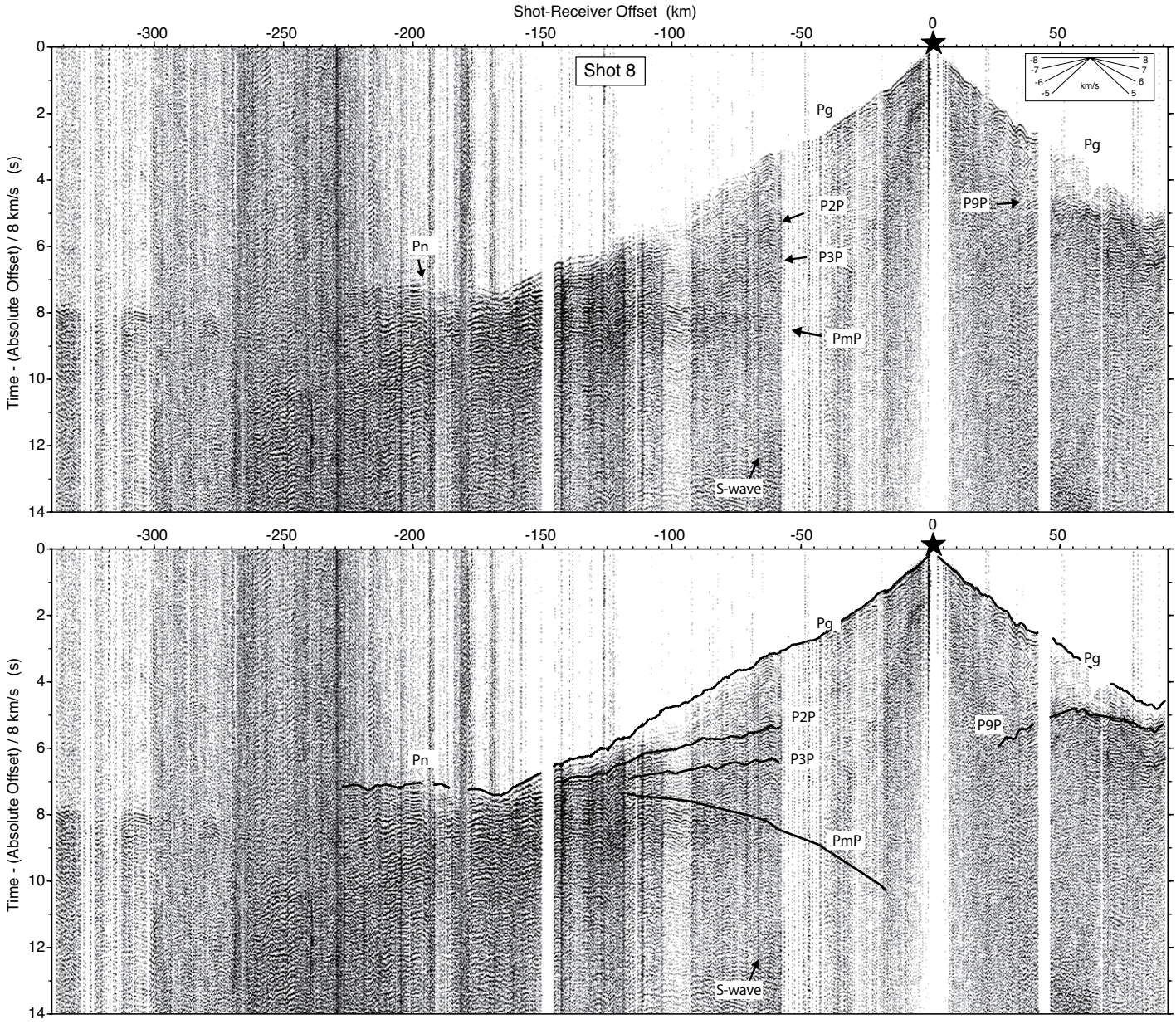

Figure 5. Seismic data shot gather for shot 8 in central Idaho with and without phase picks. Time axis is reduced at 8 km/s. Data are band-pass filtered, and trace amplitudes are normalized. See text for description of the labeled seismic arrivals.

smaller than the length of the model. Details in the velocity structure are allowed to emerge through subsequent iterations as the horizontal and vertical smoothing is reduced gradually to maintain model stability. This approach pushes traveltime misfits into large, smooth structure, such that the final model is a smooth version of the true velocity structure. A range of reasonable smoothing schemes will produce velocity models with the same major features, while the optimal scheme minimizes ray path streaking and artifacts in areas of poor ray coverage.

The layer-stripping philosophy (Parsons et al., 1996; Zelt et al., 1996; Zelt, 1999) attempts to build a robust model by using the highest-quality data first, and only incorporating lesser-quality data once the better data have been modeled. This process is accomplished by beginning with the shortest shot-receiver offset arrivals, which usually have the highest signal-to-noise ratio and the least uncertainty, and using them to model the shallowest layers of the model with the highest resolution. The short ray paths mean that high-quality traveltime misfits are only being applied to a small number of grid cells at shallow depth, which reduces uncertainty in any given cell. After this layer of the model has reached a satisfactory misfit, the shallow portion of the model is kept fixed during modeling of deeper layers. The next set of traveltimes is incorporated to model the next deeper layer, and the procedure is continued until all phases have been incorporated into the model. Larger smoothing is maintained in the deeper layers of the model as compared to the shallower layers, corresponding to the larger pick uncertainty and longer ray paths. This process forces the misfits of each phase into the deeper layers of the model that have not already been constrained by more reliable traveltimes.

TABLE 1. TRAVELTIME PICK INFORMATION BY SEISMIC PHASE

Shot number:	1	2	3	5	7	8	9	10	Picking uncertainty (ms)	RMS data misfit (ms)
X-location (km)										
	6	55	97	165	212	339	379	417	–	–
Number of traveltime picks for each phase										
Pg, all offsets	751	1414	1770	1919	1905	1296	779	738	40–120	43
Pg, high S/N	369	746	1158	1226	938	426	233	198	20–40	28
P1P	–	615	561	389	297	–	–	–	40–140	96
P2P	–	–	–	–	215	547	–	–	80–120	48
P3P	–	–	–	–	–	212	188	287	40–180	64
P4P	–	–	–	–	129	–	–	–	40	44
P5P	–	105	–	–	–	–	–	–	80	48
P6P	–	–	–	–	96	–	–	–	120	106
P7P	–	–	–	–	–	–	115	–	40	25
P8P	–	–	–	–	–	–	–	118	60	81
P9P	–	–	–	–	–	155	–	68	80–120	105
PmP-w	821	1265	1016	740	1098	–	–	–	20–140	95
PmP-e	–	–	–	–	525	522	296	577	40–300	224
Pn	782	434	406	172	185	261	-	622	120–300	169

Note: RMS—root mean square; S/N—signal-to-noise ratio.

Implementation

The orientation of the IDOR controlled-source seismic profile was approximately east-west, with road and trail access resulting in a crooked line geometry with ~40 km of north-south variation. The 3-D model box was 430 km × 45 km × 50 km, with a 500 m grid size, to allow ray tracing through the velocity volume with true shot and receiver locations. The *x*-*y* coordinate system used for the traveltime tomography was based on a Transverse Mercator coordinate system centered on −115° longitude. The *z*-axis was depth below sea level, and true shot and receiver elevations were included in the model.

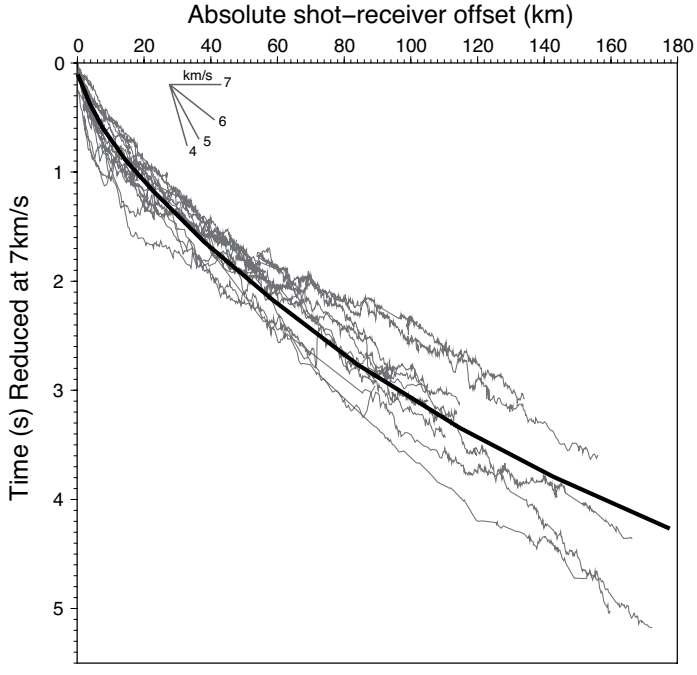

Figure 6. One-dimensional (1-D) starting velocity model (thick line) for upper-crustal tomography derived from the Pg picks for all shots (thin lines). Time axis is reduced at 7 km/s.

Upper Crust

The preferred starting model for the traveltime inversion was a very smooth one-dimensional (1-D) model with no sharp changes in velocity that was based on an average of the first-arrival traveltime picks for all shots (Fig. 6). Alternative models with a faster/slower average velocity and a higher/lower velocity gradient with depth were also tested. None of the starting models included lateral variation in velocity. All of the 1-D starting models produced final 3-D models after inversion that displayed similar structure, including a lateral velocity contrast in the upper-crust velocity.

The initial smoothing for the tomography (Hole, 1992) was 240 km in *x* and *y* and 40 km in depth. The smoothing was allowed to decrease in successive iterations while maintaining a fixed horizontal-to-vertical ratio. Several *x*-*z* ratios were tested, including 2:1, 3:1, 4:1, 5:1, and 8:1. The 4:1 horizontal-to-vertical ratio was chosen because it provided the best traveltime misfits without creating obvious artifacts in the model. This ratio also mimics the dominant shape of the ray paths, since they travel much farther horizontally than they do in depth. At most scales, the crooked line geometry did not provide enough ray coverage to constrain north-south velocity variation, so the model was forced to be two-dimensional (2-D) by smoothing across the entire model volume in the *y* direction.

Reliable ray paths from Pg traveltimes constrained the first layer of the IDOR seismic velocity model to a subsurface depth of ~10 km (Fig. 7A). Due to the shot spacing, the highest signal-to-noise and short-offset (<40 km) portion of these arrivals did not have sufficient intersecting rays to model independently as the first layer. To incorporate the higher-quality information from stations at <40 km offset, the initial Pg upper-crustal model derived from all offsets was updated by tracing the traveltimes from these stations through the model with less smoothing. For this near-surface layer alone, variation in the *y* direction was allowed due to the north-south geologic variability and crooked line at the scale of the final 2 × 2 × 1 km smoothing (Table 1). These high-resolution updates to the model reveal structures in the upper ~2 km, such as sedimentary basins, that can be correlated with known surface geology. The final root-mean-square (RMS) traveltime misfit of 43 ms for all Pg picks (Fig. 8A; Table 1),